

Article

Optical Parametric Oscillation with Ultra-Low Power Threshold in a Dimer of Active-Passive Cavities

Bo Lu ¹, Chen-Rui Fan ¹, Jun-Yang Song ¹ and Chuan Wang ^{1,2,*} 

¹ School of Artificial Intelligence, Beijing Normal University, Beijing 100875, China; lubo@mail.bnu.edu.cn (B.L.); fanchenrui7@163.com (C.-R.F.); 202021210039@mail.bnu.edu.cn (J.-Y.S.)
² Beijing Academy of Quantum Information Sciences, Beijing 100193, China
* Correspondence: wangchuan@bnu.edu.cn

Abstract: Optical parametric oscillation can convert the input laser into a couple of coherent optical output with signal and idler frequencies. It is an important method for the realization of the broadband middle infrared tunable lasers. The optical parametric oscillation process depends on the ultra-fast non-linear response of matter to light with a certain pump power. Therefore, reducing the pump threshold of the optical parametric oscillation process and improving the energy conversion efficiency are of great significance to the study of non-linear optics. In this paper, we construct a dimer system that couples a passive non-linear resonator to an active resonator. Based on the dimer system, an ultra-low threshold optical parametric oscillation generation method is proposed. By coupling the gain pump mode, the non-linear effect is effectively enhanced, the pump power threshold is reduced to half of when there is no gain, and the energy conversion efficiency is increased. We believe this research provides a feasible method for a low-threshold tunable and easy-to-integrate optical parametric oscillation laser source.



Citation: Lu, B.; Fan, C.-R.; Song, J.-Y.; Wang, C. Optical Parametric Oscillation with Ultra-Low Power Threshold in a Dimer of Active-Passive Cavities. *Crystals* **2021**, *11*, 566. <https://doi.org/10.3390/cryst11050566>

Academic Editors: Da-Quan Yang, Fei Xu and Jin-Hui Chen

Received: 28 April 2021
Accepted: 17 May 2021
Published: 19 May 2021

Publisher's Note: MDPI stays neutral with regard to jurisdictional claims in published maps and institutional affiliations.



Copyright: © 2021 by the authors. Licensee MDPI, Basel, Switzerland. This article is an open access article distributed under the terms and conditions of the Creative Commons Attribution (CC BY) license (<https://creativecommons.org/licenses/by/4.0/>).

Keywords: optical parametric oscillation; optical dimer; threshold

1. Introduction

The optical parametric oscillator converts the input pump laser light into two output lights with lower frequency (usually called signal light and idler light) through the second-order nonlinear optical interaction. Specifically, the optical parametric oscillations (OPO) describes the non-linear process that occurs when the pump light passes through the $\chi^{(2)}$ material in the optical resonator, which converts a pump photon with frequency ω_p into a signal photon with frequency ω_s and an idler photon with frequency ω_i under the phase matching conditions [1–6]. In the field of quantum optics and quantum information science, the OPOs are often used as the coherent light source to generate the optical squeezed states [7], entangled photon pairs [8–12], or the correlated optical network [13].

Similarly to other non-linear optical effects, the OPOs process also has a power threshold due to the optical loss and modal phase matching condition of the materials [14]. For example, OPO thresholds have been observed in bulk lithium niobate whispering gallery resonators with 6 μ W [15], milliwatt-level OPOs thresholds have been observed in the planar periodically polarized Ti:LiNbO₃ waveguide [16]. Additionally, the thresholds of OPOs were observed in GaAs [17] and GaAs/AlGaAs [18] ridge waveguides are of 5.7 W and 210 mW, respectively. In order to improve the performance of the OPOs, the method by reducing the optical loss of the material is always considered as an important and efficient way. Relying on the specific optical device with low optical loss and field enhancement, such as the optical microcavities, the threshold of the optical non-linear effects could be improved [19,20]. Here in this study, we intend to propose a novel platform based on the whispering gallery mode (WGM) optical microcavities to show the better performance of OPOs. The WGM optical microcavity describes the optical dielectric resonator under the rotational symmetry which is the optical analogue of whispering gallery in acoustics [21].

Due to the special structure, the optical field could be totally reflected by the inner surface and the WGM microcavity usually shows a high quality factor, as the fields are resonantly enhanced in it. Recently, the studies of optical microcavities with ultra-high quality factor have been made remarkable progress in the field of light-matter interaction [22,23]. Due to the ultra-high quality factor and a small mode volume, it can greatly enhance the non-linear interaction. During the past few decades, various studies have been made based on WGM microcavities in the field of non-linear effects, such as the second harmonics [24–26], the OPOs [15,27], the photon blockade [28–30], and optical frequency combs [31,32].

In addition, the photonic molecule structure could be realized by coupling the two WGM microcavities [33]. Moreover, if we choose an active microcavity with optical gain provided to a dissipative microcavity, by properly choosing the optical gain and loss, the optical dimer with parity-time (PT) symmetry could be obtained [34,35]. Employing the parity-time symmetry, the low threshold PT-symmetric lasers could be realized [36–40]. Additionally, in the field of non-linear optics, the low optical loss may significantly enhance the non-linear effect and improve the performances of high-order sideband generation [41] and the second harmonic generation [42]. As the field distribution in the PT-symmetric structure is sensitive to the environment, it can also be used as the ultra-sensitive detector for nanoparticles [43–46].

Here in this paper, we propose a dimer system in which a passive WGM resonator made by the material with second-order non-linear coefficient $\chi^{(2)}$ is coupled with an active resonator with optical gains. The system works in the OPOs regime by a visible light pumping to produce infrared signal and idler photon pairs. The OPOs process is theoretically studied, the threshold power and the spectrum are both obtained numerically. We find that by tuning the coupling strength between the resonators, due to the energy exchange between the gain cavity and the dissipative cavity, the pump power threshold can be effectively reduced and the energy conversion efficiency can be increased. Compared with previous results, our research has greatly improved the non-linear conversion efficiency.

2. The Theoretical Model

The model for optical parametric oscillation generation is a dimer configuration of coupled passive-active microresonators, as shown in Figure 1. The second-order non-linearity in the optical passive (loss) resonator is denoted as $\chi^{(2)}$, a visible pump laser (represented by \hat{a}) at an angular frequency ω_a pumps the microresonator. We consider the degenerate OPOs process which produces a degenerate signal photon pair (represented by \hat{b}) with frequency $\omega_b = \omega_a/2$, and this process satisfies the energy-conservation and phase matching condition. Here, the coupling strength between the pump photon and signal photon under the second-order non-linearity is denoted by g . Meanwhile, an additional single-mode active micro-resonator (denoted as mode \hat{c} , with frequency $\omega_c \simeq \omega_a$) is used to evanescently coupled to the pump mode \hat{a} of the passive micro-resonator via their spectral mode overlap, with the coupling strength J .

The system with the pump laser driving under the frequency $\omega_p \simeq \omega_a$ can be described by the Hamiltonian:

$$\hat{H} = \hat{H}_0 + \hat{H}_{ab} + \hat{H}_{ac} + \hat{H}_d. \quad (1)$$

Here, \hat{H}_0 is the energy of the total three cavity modes without considering the coupling between modes, it can be expressed as

$$\hat{H}_0 = \hbar\omega_a\hat{a}^\dagger\hat{a} + \hbar\omega_b\hat{b}^\dagger\hat{b} + \hbar\omega_c\hat{c}^\dagger\hat{c}, \quad (2)$$

where $\hat{a}^\dagger(\hat{a})$, $\hat{b}^\dagger(\hat{b})$, and $\hat{c}^\dagger(\hat{c})$ are the bosonic creation (annihilation) operators of the pump, signal, and active optical modes, respectively.

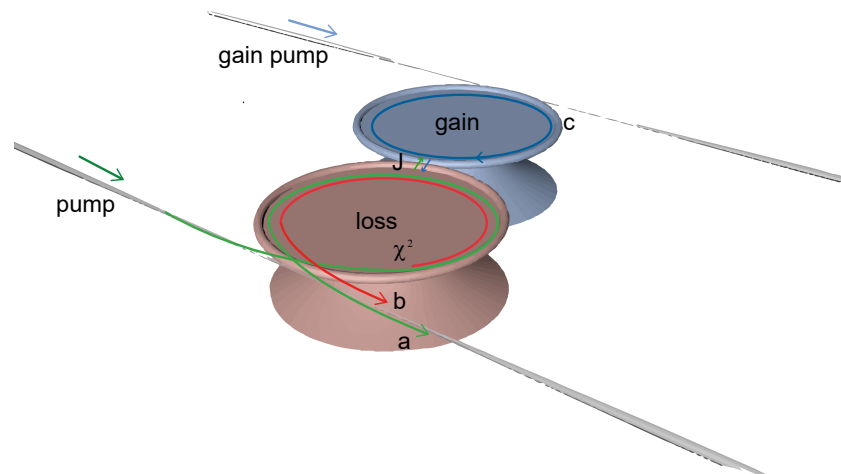


Figure 1. Schematic of a dimer with two active-passive micro-resonators to enhance the OPOs process. An optical passive (loss) micro-resonator with the second-order non-linearity $\chi^{(2)}$ (the red one), which has an input pump mode (frequency ω_a) and a signal mode (frequency $\omega_b \simeq \omega_a/2$) generated by the pump laser through the optical parametric oscillation process. Meanwhile, the pump laser in the passive micro-resonator is coupled into the active micro-resonator (the blue one) with coupling strength J . The pump laser ($\omega_p \simeq \omega_a$) drives the passive micro-resonator through the two fiber tapers.

And \hat{H}_{ab} represents the interaction between the pump photon and the signal photons in the lossy micro-resonator which can be expressed as

$$\hat{H}_{ab} = \hbar g(\hat{a}^\dagger \hat{b}^2 + \hat{a}(\hat{b}^\dagger)^2), \tag{3}$$

where g is the coupling strength between mode \hat{a} and \hat{b} due to the non-linearity $\chi^{(2)}$ which can be expressed as:

$$g = \frac{\hbar \omega_a^3 \chi^{(2)2}}{8\pi \epsilon_0 R n_{eff}^6} \zeta^2, \tag{4}$$

where n_{eff} is the refractive index of the phase-matched pump and signal modes, $\chi^{(2)}$ is the intensity of second-order non-linear coefficient of the materials, ϵ_0 is vacuum permittivity, and R is the radius of the passive micro-resonator. ζ denotes the effective mode overlap factor on the cross-section of the micro-resonator.

The third item \hat{H}_{ac} describes the mutual coupling between the pump photons in the passive micro-resonator and the single mode photons of the active micro-resonator, in the form

$$\hat{H}_{ac} = \hbar J(\hat{a}^\dagger \hat{c} + \hat{a} \hat{c}^\dagger), \tag{5}$$

where J represents the coupling strength which can be controlled by tuning the distance between the two micro-resonators.

Finally, the last item $\hat{H}_d = \hbar \sqrt{\kappa_{a,1}}(\epsilon_p \hat{a}^\dagger e^{-i\omega_p t} + \epsilon_p^* \hat{a} e^{i\omega_p t})$ describes the external driving field, in which the pump frequency ω_p , the pump amplitude ϵ_p , and the pump power P_p satisfy the relationship $\epsilon_p = \sqrt{P_p / (\hbar \omega_a)}$. The loss of the micro-resonator can be described by $\kappa_{a(b,c)} = \kappa_{(a(b,c),0)} + \kappa_{(a(b,c),1)}$, $\kappa_{(a(b,c),0)}$ represents the inherent dissipation of the micro-resonator and $\kappa_{(a(b,c),1)}$ represents the coupling dissipation between the micro-resonator and the fiber taper, in which $\kappa_{(a(b),0)} > 0$ for the lossy cavity and $\kappa_{(c,0)} < 0$ for the gain

cavity. By applying the unitary evolution operation $\hat{U}(t) = \exp[-i\omega_p(2\hat{a}^\dagger\hat{a} + \hat{b}^\dagger\hat{b} + \hat{c}^\dagger\hat{c})t]$ and regarding \hbar as 1, the total Hamiltonian of the system becomes

$$\begin{aligned} \hat{H}_{rot} = & \delta_a\hat{a}^\dagger\hat{a} + \delta_b\hat{b}^\dagger\hat{b} + \delta_c\hat{c}^\dagger\hat{c} + g[\hat{a}(\hat{b}^\dagger)^2 + \hat{a}^\dagger(\hat{b})^2] \\ & + J(\hat{a}^\dagger\hat{c} + \hat{a}\hat{c}^\dagger) + \sqrt{\kappa_{a,1}}(\varepsilon_p\hat{a}^\dagger + \varepsilon_p^*\hat{a}). \end{aligned} \quad (6)$$

where $\delta_a = \omega_a - \omega_p$, $\delta_b = \omega_b - 2\omega_p$, and $\delta_c = \omega_c - \omega_p$ represents the frequency detunings of the input modes, signal modes, and active cavity modes from the pump laser, respectively. By considering the addition of dissipation and neglecting the quantum noise term, the dynamics of the bosonic operators can be expressed as:

$$\frac{d}{dt}a = (-i\delta_a - \kappa_a)a - igb^2 - iJc - i\varepsilon_p, \quad (7)$$

$$\frac{d}{dt}b = (-i\delta_b - \kappa_b)b - 2igab^*, \quad (8)$$

$$\frac{d}{dt}c = (-i\delta_c - \kappa_c)c - iJa, \quad (9)$$

where κ_a , κ_b , and κ_c are the decay rates of the input modes, signal modes, and active cavity modes, respectively. Under the non-depletion and omit the weaker signal modes effects terms, we solve the equations under the steady-state approximations as

$$c = \frac{iJa}{-i\delta_c - \kappa_c}, \quad (10)$$

$$a = \alpha = \frac{-i\delta_c - \kappa_c}{(-i\delta_c - \kappa_c)(-i\delta_a - \kappa_a) + J^2} \sqrt{\frac{2\kappa_{a,1}P_p}{\hbar\omega_p}}. \quad (11)$$

Then, the dynamics of b can be expressed as

$$\frac{d}{dt}b = (-i\delta_b - \kappa_b)b - 2ig\alpha b^* - i\sqrt{2\kappa_b}b_{in}, \quad (12)$$

$$\frac{d}{dt}b^* = (i\delta_b - \kappa_b)b - 2ig\alpha b + i\sqrt{2\kappa_b}b_{in}^*, \quad (13)$$

where b_{in} describes the vacuum noise. By performing the Fourier transformation, the operators in time domain can be transformed into the frequency domain as

$$\frac{d}{dt}b(\omega) = \frac{i\sqrt{2\kappa_b}[-i(\delta_b - \omega) - \kappa_b]b_{in}(\omega) + 2g\alpha\sqrt{2\kappa_b}b^*(-\omega)}{[-i(\delta_b + \omega) - \kappa_b][i(\delta_b - \omega) - \kappa_b] - 4g^2\alpha^2}, \quad (14)$$

$$\frac{d}{dt}b^*(\omega) = \frac{i\sqrt{2\kappa_b}[-i(\delta_b - \omega) - \kappa_b]b_{in}^*(\omega) + 2g\alpha\sqrt{2\kappa_b}b(-\omega)}{[-i(\delta_b - \omega) - \kappa_b][i(\delta_b + \omega) - \kappa_b] - 4g^2\alpha^2}. \quad (15)$$

As the spectrum density around mode b satisfies $S_b(\omega, \omega') = 2\kappa_{b,1}\langle b^\dagger(\omega)b(\omega') \rangle$, we finally obtain:

$$\begin{aligned} S_b(\omega, \omega') = & \frac{1}{2\pi} \cdot 2\kappa_{b,1} \\ & \cdot \frac{2g\alpha\sqrt{2\kappa_a}}{[-i(\delta_b - \omega) - \kappa_b][i(\delta_b + \omega) - \kappa_b] - 4g^2\alpha^2} \\ & \cdot \frac{2g\alpha\sqrt{2\kappa_a}}{[-i(\delta_b + \omega') - \kappa_b][i(\delta_b + \omega') - \kappa_b] - 4g^2\alpha^2}. \end{aligned} \quad (16)$$

We choose the condition where the input pump power falls below the threshold of the OPOs: $(\delta_b^2 + \kappa_b^2) \gg 4g^2\alpha$. By neglecting the $4g^2\alpha$ term in the denominator, the signal spectrum density $S_b(\omega)$ becomes

$$S_b(\omega) \simeq \frac{\kappa_{b,1}(2g\alpha\sqrt{2\kappa_b})^2}{\pi\{-i(\delta_b - \omega) - \kappa_b\}[i(\delta_b + \omega) - \kappa_b]} \quad (17)$$

and the total generation rate of the signal photons could be expressed as:

$$\begin{aligned} R &= \int d\omega S_b(\omega) \\ &= \frac{4g^2\kappa_b}{\delta_b^2 + \kappa_b^2} \frac{2\kappa_{a,1}P_a}{\hbar\omega_p} \left[\frac{i\delta_c + \kappa_c}{(i\delta_c + \kappa_c)(i\delta_a + \kappa_a) + J^2} \right]^2. \end{aligned} \quad (18)$$

The pump threshold for OPOs satisfies the relation that the signal photon generation rate is larger than the loss of the signal mode, so the pump threshold could be expressed as

$$P_{th} = \frac{\hbar\omega_a(\delta_b^2 + \kappa_b^2)[(i\delta_c + \kappa_c)(i\delta_a + \kappa_a) + J^2]^2}{8g^2\kappa_{a,1}\kappa_c^2}. \quad (19)$$

When the system meets the resonant condition as $(\delta_{a(b,c)} = 0)$, we have

$$P_{th} = \frac{(\kappa_a\kappa_b + \kappa_b J^2 / \kappa_c)^2}{8\kappa_{a,1}g^2} \hbar\omega_a. \quad (20)$$

Meanwhile, according to Equations (8) and (9), we can obtain

$$b = \frac{2igab^*}{-i\delta_b - \kappa_b}, \quad (21)$$

$$a = \frac{-i\delta_b - \kappa_b}{2ig} e^{2i\theta}. \quad (22)$$

By substituting the Equations (21) and (22) into Equation (9), under resonance conditions $(\delta_{a(b,c)} = 0)$ we can get

$$|b|^2 = \frac{\sqrt{2\kappa_{a,1}a_{in}}}{g} - \frac{\kappa_b J^2 + \kappa_a\kappa_b\kappa_c}{2g^2\kappa_c}. \quad (23)$$

If we define the single-photon cooperativity as

$$\frac{1}{C_0} = \frac{\kappa_b J^2 / \kappa_c + \kappa_a\kappa_b}{2g^2} = \frac{4\kappa_{a,1}P_{th}}{\hbar\omega_a(\kappa_b J^2 / \kappa_c + \kappa_a\kappa_b)}. \quad (24)$$

Then, Equation (23) can be re-written as

$$|b|^2 = \frac{1}{C_0} \left(\sqrt{\frac{P_p}{P_{th}}} - 1 \right). \quad (25)$$

Therefore, the power of the signal photons could be solved as:

$$\begin{aligned} P_s &= 2\kappa_{b,1}\hbar\omega_b|b|^2 = \frac{2\kappa_{b,1}\hbar\omega_b}{C_0} \left(\sqrt{\frac{P_p}{P_{th}}} - 1 \right) \\ &= \frac{4\kappa_{a,1}\kappa_{b,1}}{\kappa_b(J^2/\kappa_c + \kappa_a)} (\sqrt{P_p P_{th}} - P_{th}). \end{aligned} \quad (26)$$

3. Results and Discussion for Enhanced Opos

OPOs has been experimentally studied in various materials, such as in periodically polarized lithium niobate waveguide (PPLN) [15], aluminum nitride (AlN) microcavities [27], and photonic crystals. For example, in Reference [27], a dual-resonant phase-matched AlN micro-ring resonator is used to demonstrate low-threshold parametric oscillations in the telecom infrared band, where the $\chi^{(2)}$ non-linearity and the coupling strength (g) of dual-band can be precisely controlled by nano-manufacturing technology.

According to the results in the previous studies, the dissipation of the pump mode is often larger than that of the signal light mode. Therefore, we assist an active micro-resonator in the system to increase the pump mode in the passive micro-resonator through the optical field coupling, to improve the performance of non-linear effects. Here we choose the parameters in our numerical simulation as, the non-linear coupling strength g produced by the $\chi^{(2)}$ non-linearity is $g/2\pi = 80$ kHz refers to the parameters obtained from the experiment in Reference [27], the pump laser mode wavelength is $\lambda_a = 780$ nm, the signal mode wavelength generated by the optical parameter oscillation process is $\lambda_b = 1560$ nm, the intrinsic optical factors Q_0 of the pump mode and the signal mode are 1.0×10^5 and 2.0×10^5 , respectively. The total quality factor Q of the pump mode and the signal mode are 2.0×10^5 and 4.0×10^5 (corresponding to the total loss rate $\kappa_a/2\pi = 1.92$ GHz, $\kappa_b/2\pi = 480$ MHz, the coupling loss rate $\kappa_{a,1}/2\pi = 960$ MHz, $\kappa_{b,1}/2\pi = 240$ MHz).

The material of the passive micro-resonator is AlN [27]. The active micro-resonator can use a thulium ion (or zirconium) doped silica resonator, and can be excited by a pump laser doped with rare earth ions to generate a gain mode, based on a micro-resonator made of $Ti : Al_2O_3$, or a tunable droplet micro-resonator based on electro-wetting [47–51]. Here we set the coupling strength as $J/2\pi = 0.8$ GHz, which can be controlled by tuning the gap distance between two micro-resonators [52]. The phase matching between the input mode a and the signal mode b in the micro-resonator can be controlled by the width of the micro-resonator roughly meet the phase matching, and fine-tuned by thermal tuning [27]. Besides, the gain modes of the active micro-resonator is to detune the signal modes of the passive micro-resonator.

To show the influence of the active (gain) micro-resonator on the OPOs process of the system. We first study the relationship between the coupling strength J and the pump power threshold (P_{th}) of OPO, based on Equation (20), and the result is shown in Figure 2.

Obviously, when $J = 0$, it is the original system without gain. Mathematically, the Equation (20) will also become the form of the OPOs pump power threshold in Reference [27], and the pump power threshold of the system without gain is about 26.3 mW. After the active cavity is coupled with the coupling strength $J = 800$ MHz and the gain mode $\kappa_c = -1$ GHz, the pump power threshold is reduced to about 11.7 mW. We found that the introduction of gain significantly reduced the OPOs threshold. In Figure 2, we find that as the coupling strength (J) increases, the pump power threshold for OPOs decreases significantly. This can be understood as the gain of the active (gain) cavity coupled to the passive (dissipative) cavity compensates for part of the dissipation and enhances the $\chi^{(2)}$ non-linear process. When we choose a larger coupling strength J , that is, by reducing the coupling distance between the two micro-resonators, we can reduce the pump power threshold for OPOs generation reduced to half of when there is no gain.

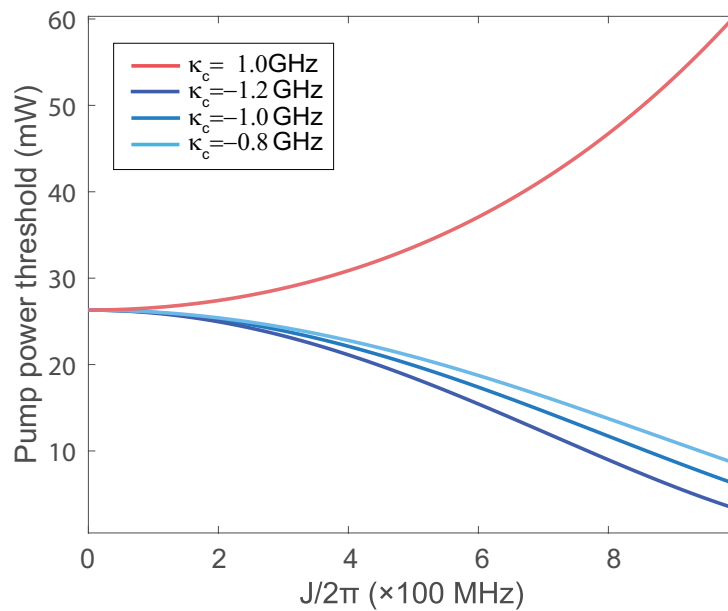


Figure 2. The pump threshold (P_{th}) of the optical parametric oscillation as a function of the coupling strength (J) between the micro-resonators, and the parameter are chosen to be $\delta_a/2\pi = 0$, $\delta_b/2\pi = 0$, $\delta_c/2\pi = 0$, $\kappa_a = 1.92$ GHz, $\kappa_b = 480$ MHz, $\kappa_{a,1} = 960$ MHz, and $g = 80$ kHz. The dark blue line, blue line, and light blue line represent the gain rate of mode c is $\kappa_c = -1.2, -1, -0.8$ GHz, respectively. The red line represents the dissipation rate of mode c is $\kappa_c = 1$ GHz.

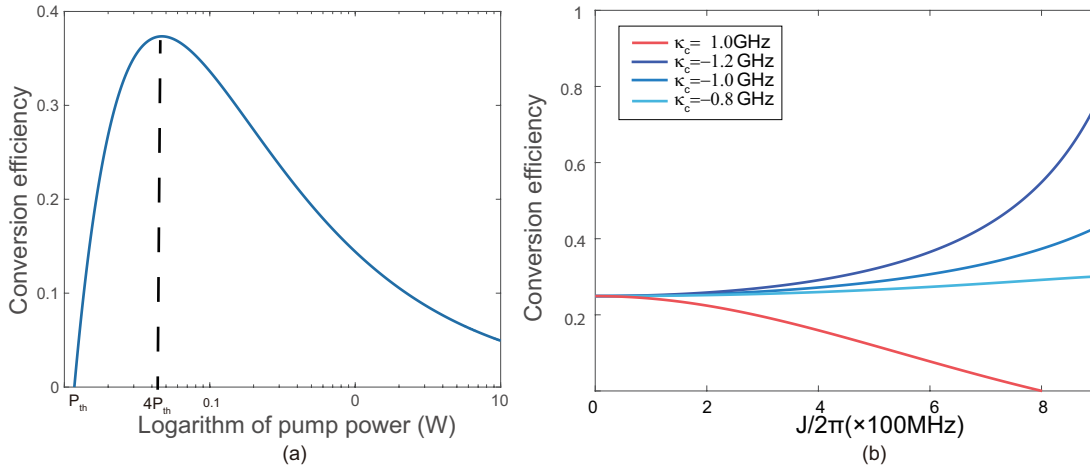


Figure 3. (a) Energy conversion efficiency η as a function of pump power P_p . The parameter $J = 800$ MHz. The dotted line is the maximum energy conversion efficiency $\eta = 37\%$, which is located at $P_p = 4P_{th}$. (b) Energy conversion efficiency η as a function of the coupling strength J . The pump power is at $P_p = 4P_{th}$. The other parameters in (a,b) are the same as in Figure 2.

By calculation of the signal light power, we found in Equation (26) that in order to generate the signal light more effectively, it is not required to increase the power of the pump source. In order to study the relationship between coupling strength and energy conversion efficiency in the OPOs process, we introduce energy conversion efficiency as

$$\eta = \frac{P_s}{P_p} = \frac{4\kappa_{a,1}\kappa_{b,1}}{\kappa_b(J^2/\kappa_c + \kappa_a)} (\sqrt{P_{th}/P_p} - P_{th}/P_p). \tag{27}$$

We present the relationship between energy efficiency and pump power, which is shown in Figure 3a.

We find that energy conversion efficiency η is related to the pump power P_p , the mode dissipation rate ($\kappa_{a(b,c)}, \kappa_{a,1(b,1)}$), and the coupling strength J . Different from the second harmonic generation process by increasing the pump power to increase the energy conversion efficiency ($J = 0, \eta = 25\%$ corresponding to Figure 3b when there is no coupling), when the pump power $4P = P_{th}$, we can obtain the maximal energy conversion efficiency $\eta = 37\%$ which is much higher than the case of no gain cavity. From Equation (27), we find that it is very effective to increase energy conversion efficiency by increasing $\kappa_{a(b),1}$ and the coupling strength J . This is of great significance to our modulate system. For example, over-coupling will not only increase the energy conversion efficiency but also increase the pump power threshold. Meanwhile, we can increase the energy conversion efficiency by increasing the coupling strength between the resonators and reduce the pump power threshold. As shown in Figure 3b, we can change the energy efficiency η by tuning the gap distance between the micro-resonators. The reason is that as the coupling strength between the resonators increases, the gain cavity compensates for the loss of mode a of the dissipative cavity. The coupling gain of the pump light field enhances the non-linear process in the dissipative cavity and improves the energy conversion efficiency of the OPOs process.

Here we only consider the case that the system is under the resonant condition in the above, and we did not consider the impact of the detuning between the pump power and modes a, b , and c on the pump power threshold. In the following, we will discuss the impact of detuning on the pump power for the system to produce the OPOs process. Equation (19) is used to calculate the pump power threshold changes in the presence of various detunings, as shown in Figure 4.

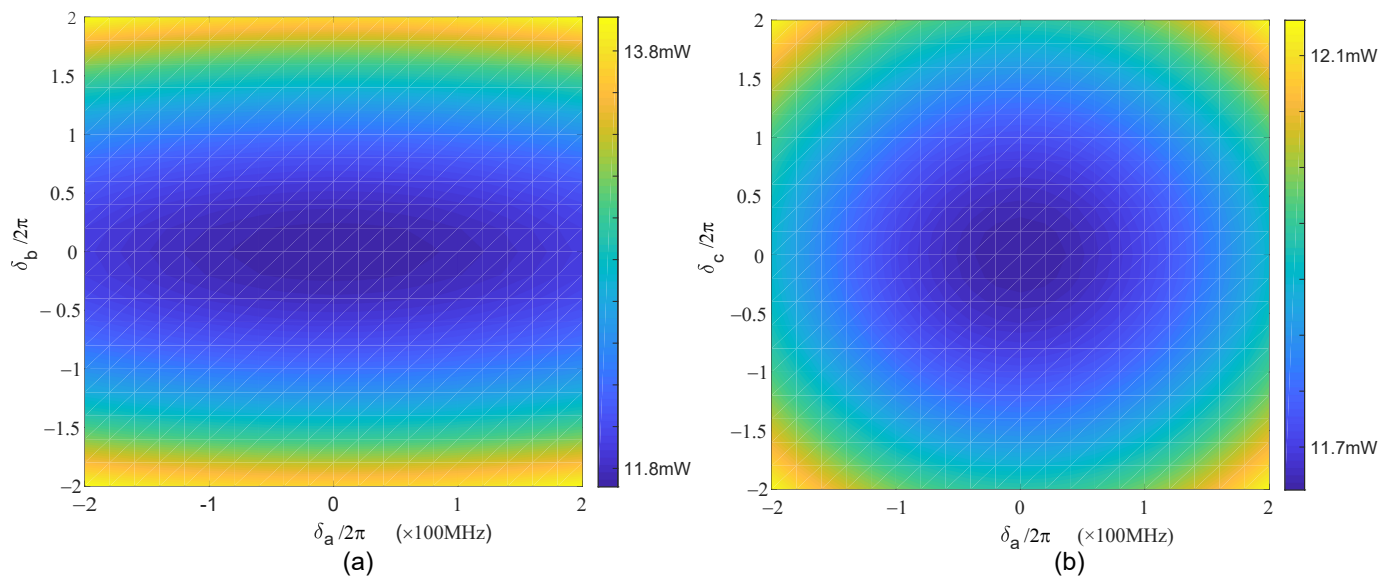


Figure 4. (a) Contour plot of power threshold as a function of the detuning δ_a between the input mode a and pump field, as well as the detuning δ_b between the signal mode b and the pump field, $\delta_a = \omega_a - \omega_p$, $\delta_b = \omega_b - 2\omega_p$, and $\delta_c = 0$. (b) Contour plot of power threshold as a function of the detuning δ_c between the gain mode c and the pump field as well as the detuning δ_a , $\delta_c = \omega_c - \omega_p$, and $\delta_b = 0$. Other parameters are $\kappa_a = 1.92$ GHz, $\kappa_b = 480$ MHz, $\kappa_c = -1$ GHz, $\kappa_{a,1} = 960$ MHz, and $g = 80$ kHz.

We find that the pump power threshold increases with the detuning, regardless of the detuning direction. This is because the interaction induced by the second-order non-linearity is weakened in the non-resonant case, and the non-resonant coupling with the gain cavity prevents the decrease in the optical field intensity in the loss cavity. These will inhibit the generation of the optical parametric oscillation process and increase the pump threshold. Therefore, in order to obtain a lower pump power threshold, it is required to put the system in resonance as much as possible.

4. Summary

In summary, we proposed a dimer system consists of a passive (dissipative) micro-resonator with $\chi^{(2)}$ non-linearity coupled with an active (gain) micro-resonator, in which the optical parametric oscillation is theoretically studied. By tuning the coupling strength between resonators, the pump power threshold that generates the OPOs process could be reduced and its energy conversion efficiency could be improved. Within the range of adjustable coupling strength, we can reduce the pump power threshold to half of the power without gain and increase its energy conversion efficiency to 37%. This work has adopted feasible technologies which greatly improve the performance of the single resonator to generate the OPOs, and it also provides a feasible way for the development of high efficiency and low threshold tunable OPOs laser source.

Author Contributions: Conceptualization, B.L. and C.W.; formal analysis, C.-R.F. and B.L.; writing—original draft preparation, B.L. and C.W.; writing—review and editing, J.-Y.S.; supervision, C.W.; project administration, C.W.; funding acquisition, C.W. All authors have read and agreed to the published version of the manuscript.

Funding: This work is supported by the National Natural Science Foundation of China through Grants Nos. 62071448; the Fundamental Research Funds for the Central Universities (BNU).

Data Availability Statement: Not applicable.

Conflicts of Interest: The authors declare no conflicts of interest.

References

1. Giordmaine, J.A.; Miller, R.C. Tunable coherent parametric oscillation in LiNbO₃ at optical frequencies. *Phys. Rev. Lett.* **1965**, *14*, 973. [[CrossRef](#)]
2. Myers, L.E.; Bosenberg, W.R. Periodically poled lithium niobate and quasi-phase-matched optical parametric oscillators. *IEEE J. Quantum Electron.* **1997**, *33*, 1663–1672. [[CrossRef](#)]
3. Powers, P.; Kulp, T.J.; Bisson, S. Continuous tuning of a continuous-wave periodically poled lithium niobate optical parametric oscillator by use of a fan-out grating design. *Opt. Lett.* **1998**, *23*, 159–161. [[CrossRef](#)]
4. Vainio, M.; Siltanen, M.; Peltola, J.; Halonen, L. Continuous-wave optical parametric oscillator tuned by a diffraction grating. *Opt. Express* **2009**, *17*, 7702–7707. [[CrossRef](#)] [[PubMed](#)]
5. Gross, P.; Klein, M.; Ridderbusch, H.; Lee, D.H.; Meyn, J.P.; Wallenstein, R.; Boller, K.J. Wide wavelength tuning of an optical parametric oscillator through electro-optic shaping of the gain spectrum. *Opt. Lett.* **2002**, *27*, 1433–1435. [[CrossRef](#)]
6. Siltanen, M.; Vainio, M.; Halonen, L. Pump-tunable continuous-wave singly resonant optical parametric oscillator from 2.5 to 4.4 μm . *Opt. Express* **2010**, *18*, 14087–14092. [[CrossRef](#)]
7. Wu, L.A.; Kimble, H.J.; Hall, J.L.; Wu, H. Generation of Squeezed States by Parametric Down Conversion. *Phys. Rev. Lett.* **1986**, *57*, 2520–2523. [[CrossRef](#)] [[PubMed](#)]
8. Morin, O.; d’Auria, V.; Fabre, C.; Laurat, J. High-fidelity single-photon source based on a Type II optical parametric oscillator. *Opt. Lett.* **2012**, *37*, 3738–3740. [[CrossRef](#)]
9. Förtsch, M.; Fürst, J.U.; Wittmann, C.; Strelakov, D.; Aiello, A.; Chekhova, M.V.; Silberhorn, C.; Leuchs, G.; Marquardt, C. A versatile source of single photons for quantum information processing. *Nat. Commun.* **2013**, *4*, 1–5. [[CrossRef](#)]
10. Vernon, Z.; Sipe, J. Strongly driven nonlinear quantum optics in microring resonators. *Phys. Rev. A* **2015**, *92*, 033840. [[CrossRef](#)]
11. Guo, X.; Zou, C.L.; Schuck, C.; Jung, H.; Cheng, R.; Tang, H.X. Parametric down-conversion photon-pair source on a nanophotonic chip. *Light. Sci. Appl.* **2017**, *6*, e16249. [[CrossRef](#)]
12. Lu, X.; Li, Q.; Westly, D.A.; Moille, G.; Singh, A.; Anant, V.; Srinivasan, K. Chip-integrated visible–telecom entangled photon pair source for quantum communication. *Nat. Phys.* **2019**, *15*, 373–381. [[CrossRef](#)] [[PubMed](#)]
13. Yamamoto, Y.; Aihara, K.; Leleu, T.; Kawarabayashi, K.i.; Kako, S.; Fejer, M.; Inoue, K.; Takesue, H. Coherent Ising machines—Optical neural networks operating at the quantum limit. *NPJ Quantum Inf.* **2017**, *3*, 1–15. [[CrossRef](#)]
14. Breunig, I. Three-wave mixing in whispering gallery resonators. *Laser Photonics Rev.* **2016**, *10*, 569–587. [[CrossRef](#)]
15. Fürst, J.U.; Strelakov, D.V.; Elser, D.; Aiello, A.; Andersen, U.L.; Marquardt, C.; Leuchs, G. Low-Threshold Optical Parametric Oscillations in a Whispering Gallery Mode Resonator. *Phys. Rev. Lett.* **2010**, *105*, 263904. [[CrossRef](#)] [[PubMed](#)]
16. Schreiber, G.; Hofmann, D.; Grundkoetter, W.; Lee, Y.L.; Suche, H.; Quiring, V.; Ricken, R.; Sohler, W. Nonlinear integrated optical frequency converters with periodically poled Ti: LiNbO₃ waveguides. In Proceedings of the Integrated Optics Devices V. International Society for Optics and Photonics, San Jose, CA, USA, 23–25 January 2001; Volume 4277, pp. 144–160.
17. Oron, M.B.; Blau, P.; Pearl, S.; Katz, M. Optical parametric oscillation in orientation patterned GaAs waveguides. In *Nonlinear Frequency Generation and Conversion: Materials, Devices, and Applications XI*; Vodopyanov, K.L., Ed.; International Society for Optics and Photonics, SPIE: Bellingham, WA, USA, 2012; Volume 8240, pp. 54–64. [[CrossRef](#)]

18. Savanier, M.; Ozanam, C.; Lanco, L.; Lafosse, X.; Andronico, A.; Favero, I.; Ducci, S.; Leo, G. Near-infrared optical parametric oscillator in a III-V semiconductor waveguide. *Appl. Phys. Lett.* **2013**, *103*, 261105. [[CrossRef](#)]
19. Yang, D.; Wang, A.; Chen, J.-H.; Yu, X.-C.; Lan, C.; Ji, Y.; Xiao, Y.-F. Real-time monitoring of hydrogel phase transition in an ultrahigh Q microbubble resonator. *Photonics Res.* **2020**, *8*, 497–502. [[CrossRef](#)]
20. Yang, D.; Liu, X.; Li, X.; Duan, B.; Wang, A.; Xiao, Y. Photonic crystal nanobeam cavity devices for on-chip integrated silicon photonics. *J. Semicond.* **2021**, *42*, 023103. [[CrossRef](#)]
21. Armani, D.; Kippenberg, T.; Spillane, S.; Vahala, K. Ultra-high-Q toroid microcavity on a chip. *Nature* **2003**, *421*, 925–928. [[CrossRef](#)]
22. Dayan, B.; Parkins, A.; Aoki, T.; Ostby, E.; Vahala, K.; Kimble, H. A photon turnstile dynamically regulated by one atom. *Science* **2008**, *319*, 1062–1065. [[CrossRef](#)] [[PubMed](#)]
23. Carmon, T.; Yang, L.; Vahala, K.J. Dynamical thermal behavior and thermal self-stability of microcavities. *Opt. Express* **2004**, *12*, 4742–4750. [[CrossRef](#)]
24. Guo, X.; Zou, C.L.; Tang, H.X. Second-harmonic generation in aluminum nitride microrings with 2500%/W conversion efficiency. *Optica* **2016**, *3*, 1126–1131. [[CrossRef](#)]
25. Xiong, C.; Pernice, W.; Ryu, K.K.; Schuck, C.; Fong, K.Y.; Palacios, T.; Tang, H.X. Integrated GaN photonic circuits on silicon (100) for second harmonic generation. *Opt. Express* **2011**, *19*, 10462–10470. [[CrossRef](#)] [[PubMed](#)]
26. Pernice, W.; Xiong, C.; Schuck, C.; Tang, H. Second harmonic generation in phase matched aluminum nitride waveguides and micro-ring resonators. *Appl. Phys. Lett.* **2012**, *100*, 223501. [[CrossRef](#)]
27. Bruch, A.W.; Liu, X.; Surya, J.B.; Zou, C.L.; Tang, H.X. On-chip χ (2) microring optical parametric oscillator. *Optica* **2019**, *6*, 1361–1366. [[CrossRef](#)]
28. Miranowicz, A.; Paprzycka, M.; Liu, Y.x.; Bajer, J.; Nori, F. Two-photon and three-photon blockades in driven nonlinear systems. *Phys. Rev. A* **2013**, *87*, 023809. [[CrossRef](#)]
29. Zhou, Y.; Shen, H.; Yi, X. Unconventional photon blockade with second-order nonlinearity. *Phys. Rev. A* **2015**, *92*, 023838. [[CrossRef](#)]
30. Roberts, D.; Clerk, A.A. Driven-dissipative quantum Kerr resonators: New exact solutions, photon blockade and quantum bistability. *Phys. Rev. X* **2020**, *10*, 021022.
31. Kippenberg, T.J.; Holzwarth, R.; Diddams, S.A. Microresonator-Based Optical Frequency Combs. *Science* **2011**, *332*, 555–559. [[CrossRef](#)] [[PubMed](#)]
32. Chen, H.J.; Ji, Q.X.; Wang, H.; Yang, Q.F.; Cao, Q.T.; Gong, Q.; Yi, X.; Xiao, Y.F. Chaos-assisted two-octave-spanning microcombs. *Nat. Commun.* **2020**, *11*, 1–6. [[CrossRef](#)]
33. Gao, Y.P.; Sun, Y.; Liu, X.F.; Wang, T.J.; Wang, C. Parity-Time-Anyonic Coupled Resonators System With Tunable Exceptional Points. *IEEE Access* **2019**, *7*, 107874–107878. [[CrossRef](#)]
34. Peng, B.; Özdemir, Ş.K.; Lei, F.; Monifi, F.; Gianfreda, M.; Long, G.L.; Fan, S.; Nori, F.; Bender, C.M.; Yang, L. Parity-time-symmetric whispering-gallery microcavities. *Nat. Phys.* **2014**, *10*, 394–398. [[CrossRef](#)]
35. Konotop, V.V.; Yang, J.; Zezyulin, D.A. Nonlinear waves in PT-symmetric systems. *Rev. Mod. Phys.* **2016**, *88*, 035002. [[CrossRef](#)]
36. Feng, L.; Wong, Z.J.; Ma, R.M.; Wang, Y.; Zhang, X. Single-mode laser by parity-time symmetry breaking. *Science* **2014**, *346*, 972–975. [[CrossRef](#)]
37. Hodaei, H.; Miri, M.A.; Heinrich, M.; Christodoulides, D.N.; Khajavikhan, M. Parity-time-symmetric microring lasers. *Science* **2014**, *346*, 975–978. [[CrossRef](#)] [[PubMed](#)]
38. Chang, L.; Jiang, X.; Hua, S.; Yang, C.; Wen, J.; Jiang, L.; Li, G.; Wang, G.; Xiao, M. Parity-time symmetry and variable optical isolation in active-passive-coupled microresonators. *Nat. Photonics* **2014**, *8*, 524–529. [[CrossRef](#)]
39. Hodaei, H.; Miri, M.A.; Hassan, A.U.; Hayenga, W.; Heinrich, M.; Christodoulides, D.; Khajavikhan, M. Parity-time-symmetric coupled microring lasers operating around an exceptional point. *Opt. Lett.* **2015**, *40*, 4955–4958. [[CrossRef](#)]
40. Hodaei, H.; Miri, M.A.; Hassan, A.U.; Hayenga, W.E.; Heinrich, M.; Christodoulides, D.N.; Khajavikhan, M. Single mode lasing in transversely multi-moded PT-symmetric microring resonators. *Laser Photonics Rev.* **2016**, *10*, 494–499. [[CrossRef](#)]
41. Jiao, Y.; Lü, H.; Qian, J.; Li, Y.; Jing, H. Nonlinear optomechanics with gain and loss: Amplifying higher-order sideband and group delay. *New J. Phys.* **2016**, *18*, 083034. [[CrossRef](#)]
42. Li, J.; Yu, R.; Qu, Y.; Ding, C.; Zhang, D.; Wu, Y. Second-harmonic generation with ultralow-power pump thresholds in a dimer of two active-passive cavities. *Phys. Rev. A* **2017**, *96*, 013815. [[CrossRef](#)]
43. Özdemir, Ş.K.; Zhu, J.; Yang, X.; Peng, B.; Yilmaz, H.; He, L.; Monifi, F.; Huang, S.H.; Long, G.L.; Yang, L. Highly sensitive detection of nanoparticles with a self-referenced and self-heterodyned whispering-gallery Raman microlaser. *Proc. Natl. Acad. Sci. USA* **2014**, *111*, E3836–E3844. [[CrossRef](#)] [[PubMed](#)]
44. Zhi, Y.; Yu, X.C.; Gong, Q.; Yang, L.; Xiao, Y.F. Single nanoparticle detection using optical microcavities. *Adv. Mater.* **2017**, *29*, 1604920. [[CrossRef](#)]
45. Zhu, J.; Ozdemir, S.K.; Xiao, Y.F.; Li, L.; He, L.; Chen, D.R.; Yang, L. On-chip single nanoparticle detection and sizing by mode splitting in an ultrahigh-Q microresonator. *Nat. Photonics* **2010**, *4*, 46. [[CrossRef](#)]
46. Jin, X.-X.; Gao, Y.-P.; Zheng, S.-H.; Wang, T.-J.; Wang, C. The Particle Induced Mode Splitting and Exceptional Points in Whispering-Gallery Mode Microcavity. *IEEE Photonics J.* **2020**, *12*, 1–14. [[CrossRef](#)]

47. Mehrabani, S.; Armani, A.M. Blue upconversion laser based on thulium-doped silica microcavity. *Opt. Lett.* **2013**, *38*, 4346–4349. [[CrossRef](#)]
48. Choi, H.; Armani, A.M. High efficiency Raman lasers based on Zr-doped silica hybrid microcavities. *ACS Photonics* **2016**, *3*, 2383–2388. [[CrossRef](#)]
49. Lim, W.; Zohrabi, M.; Zhu, J.; Gopinath, J.T.; Bright, V.M. Electrowetting-Based Tunable Liquid Droplet Microresonator. In Proceedings of the 2021 IEEE 34th International Conference on Micro Electro Mechanical Systems (MEMS), Online, 25–29 January 2021; pp. 957–960. [[CrossRef](#)]
50. Boucher, Y.; Georges, P.; Brun, A.; Pocholle, J.P.; Papuchon, M. Seeding of a Ti:Al₂O₃ laser by a vertical- cavity surface-emitting-laser in the nanosecond range. In Proceedings of the Conference on Lasers and Electro-Optics, Anaheim, CA, USA, 8–13 May 1994; p. CTuK67.
51. Liu, H.; Yang, Y.; Zhang, G.; Kuo, Y.K.; Huang, M.F.; Birnbaum, M. Novel Folded-Cavity Design for a Ti:Al₂O₃ Laser. In *Advanced Solid State Lasers*. Optical Society of America; Optical Society of America: Washington, DC, USA, 1994; p. TL8. [[CrossRef](#)]
52. Peng, B.; Özdemir, Ş.K.; Zhu, J.; Yang, L. Photonic molecules formed by coupled hybrid resonators. *Opt. Lett.* **2012**, *37*, 3435–3437. [[CrossRef](#)]